


Theoretical Studies on a Rotating Film Reactor for Hydrogen Production from Methane

Tobias Becker* and David W. Agar

DOI: 10.1002/cite.202100183

 This is an open access article under the terms of the Creative Commons Attribution License, which permits use, distribution and reproduction in any medium, provided the original work is properly cited.

A film of liquid metal can protect the reactor wall from carbon deposits during methane pyrolysis, discharge carbon from the reactor and prevent blocking. The film can be generated by rotation in a rotating film reactor. Parameters such as liquid volume flow, operating mode or the diameter of the reactor can have an influence on the reaction behavior. A design of experiments was used to investigate the rotating film reactor in more detail and to characterize the influence of various parameters.

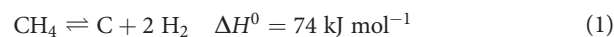
Keywords: Carbon deposition, Hydrogen, Methane pyrolysis, Reactor modeling

Received: September 30, 2021; *accepted:* March 04, 2022

1 Introduction

In the context of decarbonization of various economic sectors, hydrogen takes a central role. More than 30 countries have developed hydrogen strategies at the beginning of the year and more than 200 different hydrogen projects have been planned. [1]

The largest quantities of hydrogen are still obtained from steam reforming of methane, which produces stoichiometrically 5.5 t CO₂ per ton H₂. The pyrolysis of methane to hydrogen and solid carbon represents an alternative process. If the energy comes from renewable sources, the hydrogen can be produced CO₂-free.



Various economic studies of methane pyrolysis have found that small to medium-sized plants in particular are competitive with steam methane reforming and water electrolysis. Large plants will not become economic until taxes on CO₂ emissions have to be paid and/or carbon can be sold at a sufficient profit. [2–5]

In contrast to the economic advantages, solid carbon also creates process challenges. Carbon particles clog the catalyst pores and deactivate the catalyst [6, 7]. Regeneration by burning off the carbon is not effective since unwanted CO₂ would be produced. But thermal decomposition is also hampered by carbon formation. The investigation of different concepts such as tubular reactors, fluidized bed or moving bed reactors ended with the blocking of the reactor at walls and electrodes by carbon deposits [8–10].

In order to prevent contact between the reaction gas and the reactor wall, molten metal bubble columns in particular were studied. In addition, the carbon can be easily separated due to the difference in density to the metal [11, 12]. Plevan

et al. filled a bubble column with liquid tin at 750–900 °C for pyrolysis reaction. They found that a large part of the methane was converted in the gas phase above the liquid metal. In addition, no catalytic effect of the tin was observed [13]. Geißler et al. investigated bubble columns with fixed-bed debris, which was intended to increase the liquid phase residence time. They found no blocking by carbon during operation, only a few deposits were found between the reactor wall [14, 15]. Upham et al. studied the catalytic effect of different molten metals in a bubble column and found the largest catalytic effect for a mixture of Ni_{0.27}Bi_{0.73} [16]. The addition of another liquid salt phase showed that the carbon was almost free of metallic impurities [17]. Perez et al. investigated a bubble column with liquid gallium at 1119 °C. They figured out that part of the reaction takes place in the gas phase above the liquid, but that the gallium has a catalytic effect on the reaction. In addition, they observed carbon deposits on the walls, albeit less than when operating without liquid metal [18]. However, bubble column reactors have two main disadvantages. Firstly, the gas to liquid ratio is unfavorable for a pure gas reaction, and secondly, the residence time of the gas phase in the column is difficult to control. It depends strongly on the buoyancy force and can only significantly be influenced by internals or the height of the column.

The use of film reactors, in which only a thin film of liquid metal protects the wall, offers a solution. However,

Tobias Becker, Prof. Dr. David W. Agar
tobias4.becker@tu-dortmund.de

Technische Universität Dortmund, Fakultät Bio- und Chemieingenieurwesen, Lehrstuhl für Chemische Verfahrenstechnik, Emil-Figge Straße 66, 44227 Dortmund, Germany.

the investigation in a capillary reactor showed that due to wetting problems no formation of a wall film took place and the reactor was blocked with carbon [19,20]. Other film reactor concepts include the falling film reactor and the rotating tube reactor, where high liquid load and rotation, respectively, could ensure wetting [20].

In preliminary work, it was theoretically shown for the rotating film reactor that carbon particles with diameters larger than 50 nm hit the liquid film in 90 % of cases and do not enter the downstream piping system [21]. Based on the existing model, this work will investigate various design and operating parameters of the rotating tube reactor and their effect on methane conversion. A statistical experimental design and consideration of the effects will help to set favorable operating conditions.

2 Rotating Film Reactor Concept and Model

The operation of the rotating film reactor can be explained with reference to Fig. 1. A film of liquid tin is formed by rotation, flows through the reactor and protects the wall from carbon deposits produced by the pyrolysis reaction. The carbon floats on the film due to its lower density and is transported out of the reactor. The reactor consists of the rotating tube in the center, and two non-rotating tanks for bearing and sealing. Two operation modes of the reactor are conceivable. On the one hand, the cocurrent flow (COC) (Fig. 1 upper) where gas and liquid flow in the same

direction. On the other hand, the countercurrent (CTC) mode shown in the lower part of the figure, where gas and liquid flow in different directions. The thermal energy required for the reaction can be provided by an external heat source. In addition, there are heating and cooling zones at the inlet and outlet of the rotating pipe, so that no further reaction and carbon formation take place in the area of the non-rotating tanks.

The simulations of the rotating film reactor were made using the computational fluid dynamics (CFD) software ANSYS R19.3. Equivalent to previous studies [21], a rotationally symmetrical model was constructed. For gas phase modeling, the k - ε -RNG model with swirl-flow, production kato-launders and Menter-Lechner near-wall treatment was selected. This model showed good agreement with the experimental data of Kikuyama et al. who extensively studied the flow behavior in rotating tubes [22]. The behavior of the film was calculated separately from the CFD software and only incorporated as boundary condition. The equations of the boundary conditions can be taken in detail from previous work and are briefly summarized below. [21]

Film surface velocity w_{\max} , inner radius r_i and the constant C_1 are given by the following equations:

$$w_{\max} = \frac{1}{4} C_1 (r_i^2 - r_a^2) - \frac{1}{2} C_1 r_i^2 \log\left(\frac{r_i}{r_a}\right) \quad (2)$$

$$r_i = r_a - \delta \quad (3)$$

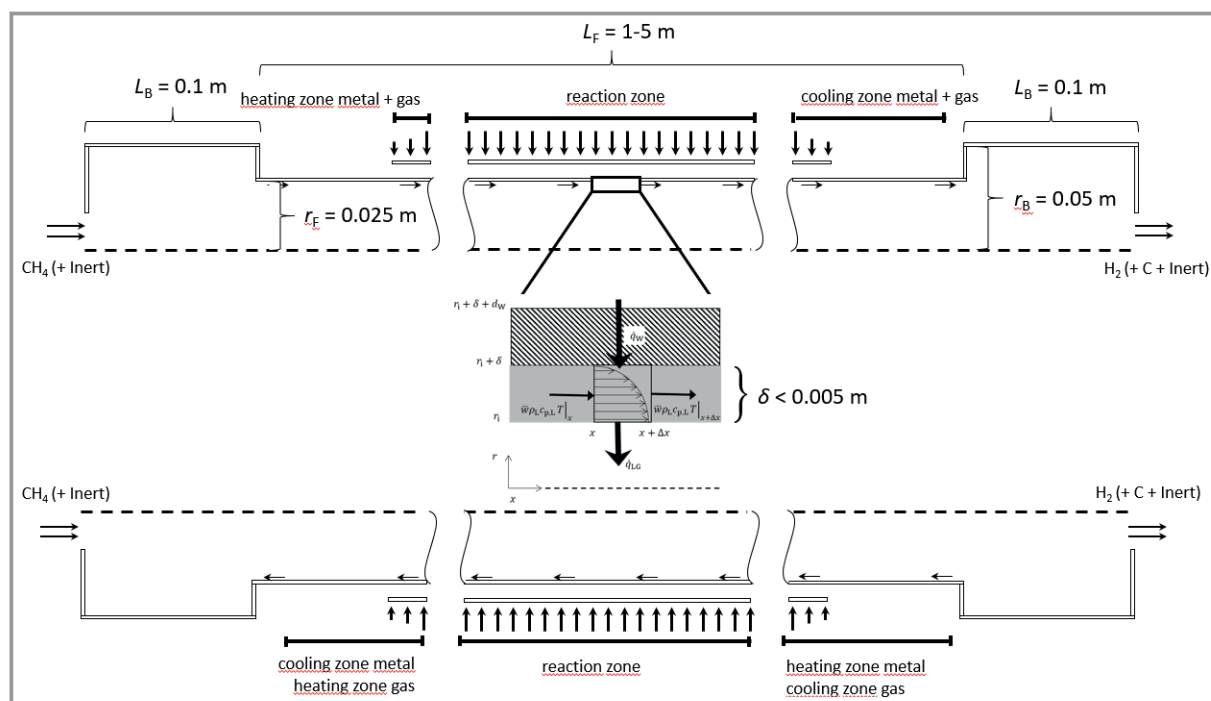


Figure 1. Functional scheme of the rotating film reactor in COC (upper) and CTC (lower) operation. Based on the cut-out element, the flow and temperature behavior of the film can be calculated.

$$C_1 = \frac{\dot{V}_L}{\pi} \left(-\frac{1}{8}r_a^4 - \frac{3}{8}r_i^4 + \frac{1}{2}r_a^2r_i^2 + \frac{1}{2}r_i^4 \log\left(\frac{r_i}{r_a}\right) \right)^{-1} \quad (4)$$

Mean film thickness is calculated from a correlation of Suppiah Singaram et al. [23]

$$\delta = \frac{1}{L_F} \int_0^{L_F} 12.45r_a \left[\frac{Re}{Re_{rot}^2} \right]^{\frac{1}{3}} \left(\frac{L_F - x}{r_a} \right)^{\frac{1}{3}} dx \quad (5)$$

$$= 9.3375 (L_F r_a^2)^{\frac{1}{3}} \left[\frac{Re}{Re_{rot}^2} \right]^{\frac{1}{3}}$$

With film Reynolds number Re and rotational Reynolds number Re_{rot}

$$Re = \frac{\dot{m}}{2\pi r_a \eta_L} \quad (6)$$

$$Re_{rot} = \frac{\omega r_a^2}{\nu} \quad (7)$$

The film temperature T_L is calculated by solving Eq. (8), which was set up according to Fig. 1:

$$\frac{\partial T_L}{\partial x} = \frac{2\pi(r_i + \delta)}{\dot{m}_L c_{pL}} \dot{q}_W - \frac{2\pi r_i}{\dot{m}_L c_{pL}} \dot{q}_{LG} \quad (8)$$

The specific heat loss due to the heating of the cold gas \dot{q}_{LG} is directly taken from ANSYS Fluent and the specific heat flow through the wall \dot{q}_W could be calculated by Eq. (9).

$$\dot{q}_W = \frac{T_{fur} - T_L}{\frac{r_i + \delta}{\lambda_w} \log\left(\frac{r_i + \delta + d_w}{r_i + \delta}\right) + \frac{1}{\alpha_{wl}}} \quad (9)$$

The gas-phase reaction was modeled using simple global kinetics of Catalán et al. [24], based on experimental data of Keipi et al. [25]

$$k(T) = k_0 T^\beta \exp\left(-\frac{E_A}{RT}\right) \quad (10)$$

$$K_C(T) = \frac{p_0}{RT} \exp\left(-\frac{\Delta_r G(T)}{RT}\right) \quad (11)$$

$$\Phi(T) = c_{CH_4}^n \left(1 - \frac{c_{H_2}^2}{c_{CH_4} K_C(T)} \right) \quad (12)$$

$$r(T) = k(T)\Phi(T) \quad (13)$$

The occurring heat sink of the endothermic pyrolysis reaction is modeled by

$$\dot{q}_R = r(T)\Delta_r H(T) \quad (14)$$

3 Design of Experiment and Ideal Plug Flow Reactor

A design of experiment (DoE) is used to investigate the influence of four different factors on the conversion. The individual factors for the DoE are shown in Tab. 1. In addition to the COC and CTC mode, the liquid volume flow \dot{V}_L , the rotation frequency rpm and the tube diameter d are to be investigated. The diameter is based on the tubes investigated by Kikuyama et al. [22]. With a correlation of Suppiah Singaram [23] the minimum rotation frequency necessary for the formation of an annular flow can be calculated. The critical value results from the smaller diameter (0.025 m) and the larger liquid volume flow (3 L min⁻¹) at $rpm = 1400$ min⁻¹, which is why 1500 min⁻¹ was selected as the lower stage.

Table 1. Varying parameters and stages of the DoE.

Parameter	Name DoE	Lower stage	Upper stage
		DoE factor -1	DoE factor 1
Operation mode	A	CTC	COC
Liquid volume flow \dot{V}_L [L min ⁻¹]	B	1	3
Rotational frequency rpm [min ⁻¹]	C	1500	3000
Diameter d [m]	D	0.025	0.05

The gas volume flows were chosen to be 3 L min⁻¹ for the small diameter and 12 L min⁻¹ for the large diameter so that the hydrodynamic residence times are identical and in order to better compare the conversions. The inlet temperature T_0 of the methane-nitrogen mixture in the ratio 9:1 is 673.15 K, since at this temperature no reaction and formation of carbon is expected yet. The reaction temperature is set to 1373.15 K, which is the maximum operating temperature of the used material, fused silica.

To ensure sufficiently high conversions, an ideal isothermal plug flow reactor is modeled first. It is expected that the conversion in the PFR will be significantly higher than in the rotating tube reactor due to non-idealities such as temperature profiles and back-mixing due to film and rotation. Therefore, 90 % should be achieved in the PFR. The balance of a volume element gives:

$$\dot{n}_{CH_4}|_z - \dot{n}_{CH_4}|_{z+\Delta z} = r\Delta V \quad (15)$$

\dot{n} describes the molar flow rate, r the reaction rate and ΔV the volume of the volume element. The reaction rate is replaced by Eq. (13). For the concentrations of methane and hydrogen c_{CH_4} and c_{H_2} , the change in the number of moles is considered. The amounts of species can be expressed as a function of conversion.

$$\begin{aligned}n_{\text{CH}_4} &= n_{\text{CH}_4,0}(1 - X) \\n_{\text{H}_2} &= n_{\text{H}_2,0} + 2n_{\text{CH}_4,0}X \\n_{\text{N}_2} &= n_{\text{N}_2,0}\end{aligned}\quad (16)$$

The concentrations are determined by means of the mole fractions by the ideal gas law.

$$c_i = \frac{n_i}{n_{\Sigma}} \frac{p}{RT} = \frac{y_i p}{RT} \quad (17)$$

n_i is the amount of substance of component i , n_{Σ} is the sum of the amounts of substance of the gas species, p is the operating pressure, R is the general gas constant and T is the temperature. Using

$$\begin{aligned}N &= \frac{n_{\Sigma 0}}{n_{\text{CH}_4,0}} \\B &= \frac{n_{\text{H}_2,0}}{n_{\text{CH}_4,0}} \\X &= \frac{n_{\text{CH}_4,0} - n_{\text{CH}_4}}{n_{\text{CH}_4,0}}\end{aligned}\quad (18)$$

and a Taylor series expansion of the left-hand side of Eq. (15), the differential equation for calculating the conversion in an isothermal tubular reactor is established.

$$\frac{p_0}{RT} \frac{u_0}{N} \frac{dX}{dz} = k(T) \left(\frac{1-X}{N+X} \right)^n \left(\frac{p_0}{RT} \right)^n \left[1 - \frac{(B+2X)^2 \frac{p_0}{RT}}{(1-X)(N+X)K_C} \right] \quad (19)$$

Using

$$x = \frac{z}{L} \quad (20)$$

$$n_{\text{H}_2,0} = 0 \Rightarrow B = 0$$

$$Da = k(T) \frac{L}{u_0} \left(\frac{p_0}{RT} \right)^{n-1}$$

finally gives

$$\frac{dX}{dx} = N Da \left(\frac{1-X}{N+X} \right)^n \left[1 - \frac{4X^2 \frac{p_0}{RT}}{(1-X)(N+X)K_C} \right] \quad (21)$$

The numerical solution of Eq. (21) is shown in Fig. 2. For a reactor length of 3 m, a conversion of about 0.87 is achieved, and for 3.5 m, 0.9. Therefore, a tube length of 3.5 m is chosen for the rotating tube reactor, where the film should reach the maximum temperature of 1373.15 K over 3 m length. This 3 m long area will be referred to as the reaction zone in the following.

4 Results

From the DoE, 16 combinations and simulations were performed. First, the simulations are evaluated as a whole to highlight the influence of certain effects. Then, the most

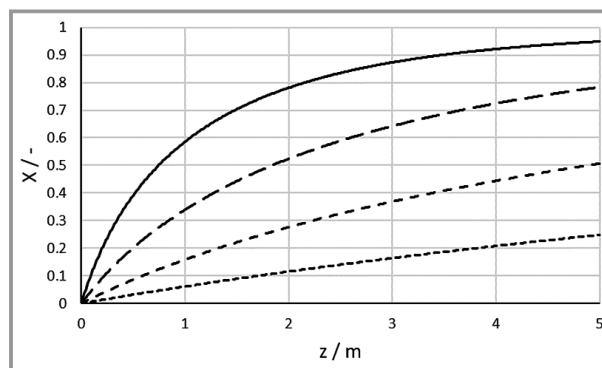


Figure 2. Pyrolysis conversion along the axial coordinate of an ideal isothermal PFR at different temperatures. (· · ·) $T = 1223.15$ K, (---) $T = 1273.15$ K, (- - -) $T = 1323.15$ K, (-) $T = 1373.15$ K.

important effects are examined and explained in more detail. The experimental design with the achieved conversion and the calculated effects is shown in Tab. 2. The single effects Ψ , as well as the double, triple and quadruple interactions have been calculated according to Siebertz et al. [26].

$$\Psi_A = \sum_{k=1}^{16} A_k X_k \quad (22)$$

$$\Psi_{AC} = \sum_{k=1}^{16} A_k C_k X_k \quad (23)$$

$$\Psi_{ABD} = \sum_{k=1}^{16} A_k B_k D_k X_k \quad (24)$$

$$\Psi_{ABCD} = \sum_{k=1}^{16} A_k B_k C_k D_k X_k \quad (25)$$

Fig. 3 shows that an increase in diameter at constant residence time leads to a significant reduction in conversion. In addition, changing from CTC to COC and increasing the rotation frequency have a positive effect on the conversion. Increasing the liquid volume flow rate seems to have only a weak decreasing effect on the conversion. Except for the dual interactions of operating mode and liquid volume flow, and rotation and diameter, the other interactions have no effect. Furthermore, all effects seem to be minor, compared to the change in diameter. The observed effects will be investigated in more detail using the flow and temperature profiles from the simulations.

4.1 Influence of the Operation Mode

Fig. 4 shows the increase in conversion for all eight cases when switching from CTC to COC. A comparison of the velocity and temperature profiles using the example of cases C and AC in Fig. 5 explains this increase in conversion. The

Table 2. DoE with stage factors, conversion and calculated effect.

No	DoE	A	B	C	D	X	Effect Ψ
1	(1)	-1	-1	-1	-1	0.63664	
2	A	1	-1	-1	-1	0.65566	0.23726
3	B	-1	1	-1	-1	0.61942	-0.03548
4	C	-1	-1	1	-1	0.63726	0.12148
5	D	-1	-1	-1	1	0.46394	-1.24500
6	AB	1	1	-1	-1	0.65707	0.08400
7	AC	1	-1	1	-1	0.66059	0.01032
8	AD	1	-1	-1	1	0.48064	-0.00704
9	BC	-1	1	1	-1	0.61849	-0.01302
10	BD	-1	1	-1	1	0.45453	0.03358
11	CD	-1	-1	1	1	0.49435	0.10510
12	ABC	1	1	1	-1	0.66064	-0.00006
13	ABD	1	1	-1	1	0.49463	0.00910
14	ACD	1	-1	1	1	0.51193	-0.00730
15	BCD	-1	1	1	1	0.48001	-0.00720
16	ABCD	1	1	1	1	0.52074	-0.00044

4.2 Influence of the Volume Flow

Fig. 6 shows that the cocurrent and countercurrent principles must be considered separately. Whereas an increase in volume flow in CTC means a loss of conversion, in COC conversion is increased. The velocity profiles in Fig. 7 explain the phenomenon.

An increase in volume flow means a higher film velocity at the wall and thus greater backflows in the CTC. In the COC, on the other hand, almost ideal plug flow is achieved. However, with a further increase in the liquid volume flow, it can be assumed that the plug profile is also destroyed in the COC and instead a backflow takes part in the reactor center (cf. Fig. 5a). It seems obvious that for COC operation there is an optimum liquid volume flow.

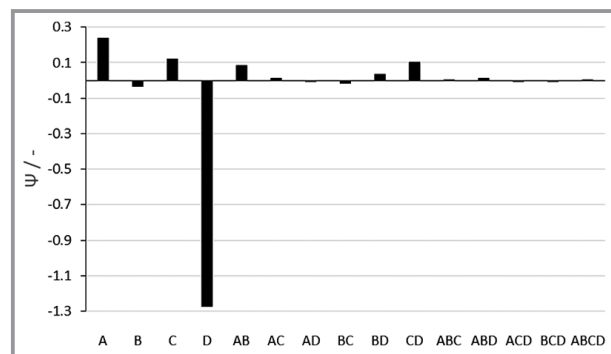


Figure 3. Resulting effects from the DoE. Positive values indicate an increase in conversion when the higher stage is set, and negative values indicate a reduction.

velocity profile in COC (Fig. 5a) is much more uniform and negative only in the center at the entrance of the reaction zone. As a result, the maximum velocity in the tube is lower and backmixing is smaller. For CTC (Fig. 5c) the backflow at the film surface results in higher axial velocities in the center of the reactor. The 300 K higher temperature at the beginning of the reaction zone (Fig. 5b and 5d) in the COC results in higher conversion.

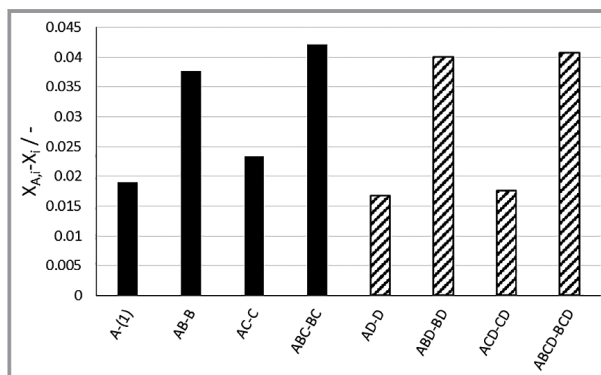


Figure 4. Change in conversion by changing the operating mode from CTC to COC (black: small diameter; stripes: large diameter).

4.3 Influence of the Rotation Frequency

For the investigated rotation frequencies, the conversion is mainly influenced at larger diameters (cf. Fig. 8). Fig. 9 shows that the increased rotation produces a somewhat more irregular flow profile (cf. Fig. 9a and 9c). However, the temperature is significantly higher over the entire reaction zone (see Fig. 9b and 9d), which is why the conversion increases despite higher mixing.

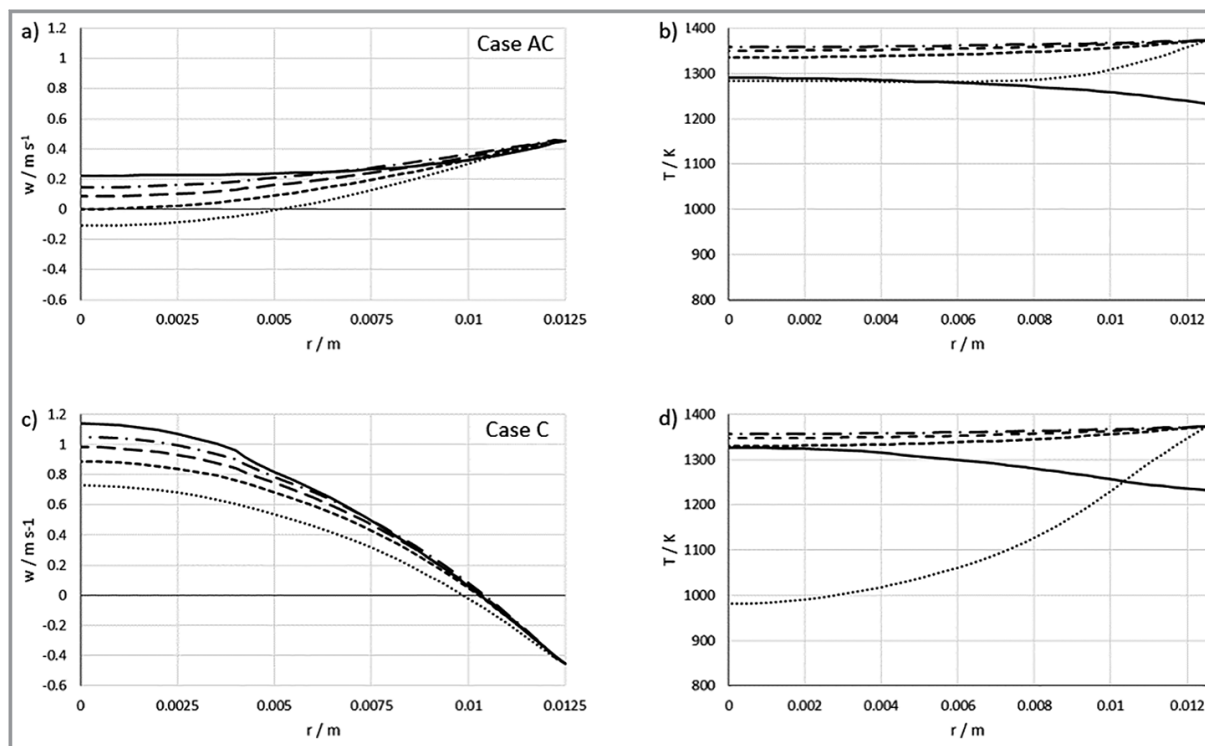


Figure 5. Radial velocity profile a) and temperature profile b) at different locations x along the reactor for COC operation and c), d) for CTC operation. $x = 0$ m to $x = 3$ m corresponds to the range of the reaction zone. (· · ·) $x = 0$ m, (---) $x = 0.75$ m, (---) $x = 1.5$ m, (- · -) $x = 2.25$ m, (-) $x = 3$ m.

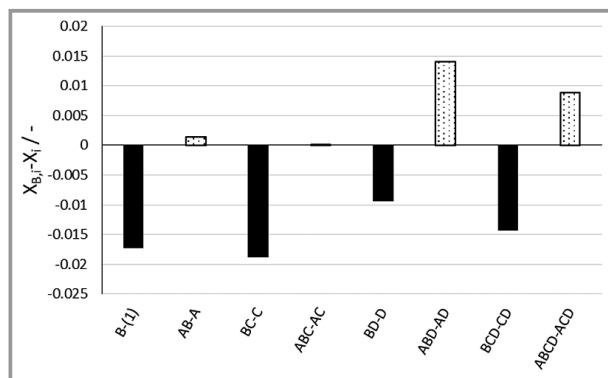


Figure 6. Changes in conversion due to increase in liquid volume flow (black: CTC; dotted: COC).

4.4 Influence of the Diameter

Fig. 10 shows the change in conversion due to an increase in diameter with a constant hydrodynamic residence time. For all cases investigated, the conversion decreases by more than 10 %. This is mainly due to the temperature profiles. A larger diameter means that the reactor heats up more slowly in the center. A comparison of the conversions as a function of temperature (cf. Fig. 2) shows that a temperature difference of 50 K can result in conversion differences of 20 %.

4.5 Comparison with Ideal Isothermal Plug Flow Reactor

To compare the rotating film reactor with the PFR, the average temperature of the reactor volume in the reaction zone is first calculated. As an example, this is done for the case AC, since the highest conversion was found there. The average temperature is 1352.69 K. The solution of Eq. (21) at this temperature gives a conversion of 79 %, which is still 13 % higher than in the rotating film reactor. This difference can be caused by non-idealities such as flow, concentration, and temperature profiles.

5 Conclusion

A rotating film reactor was investigated in more detail with a design of experiments. For a 3.5 m long reactor tube with a 3 m long reaction zone, the influence of the operating mode (CTC or COC), the liquid volume flow rate, the rotation frequency and the diameter on the conversion was investigated at a constant hydrodynamic residence time of approx. 14 s. The COC mode is used to increase the conversion by 1.5–4 % in the investigated operating range. When increasing the liquid volume flow, the CTC and COC must be considered separately. In CTC, increasing the volume flow rate

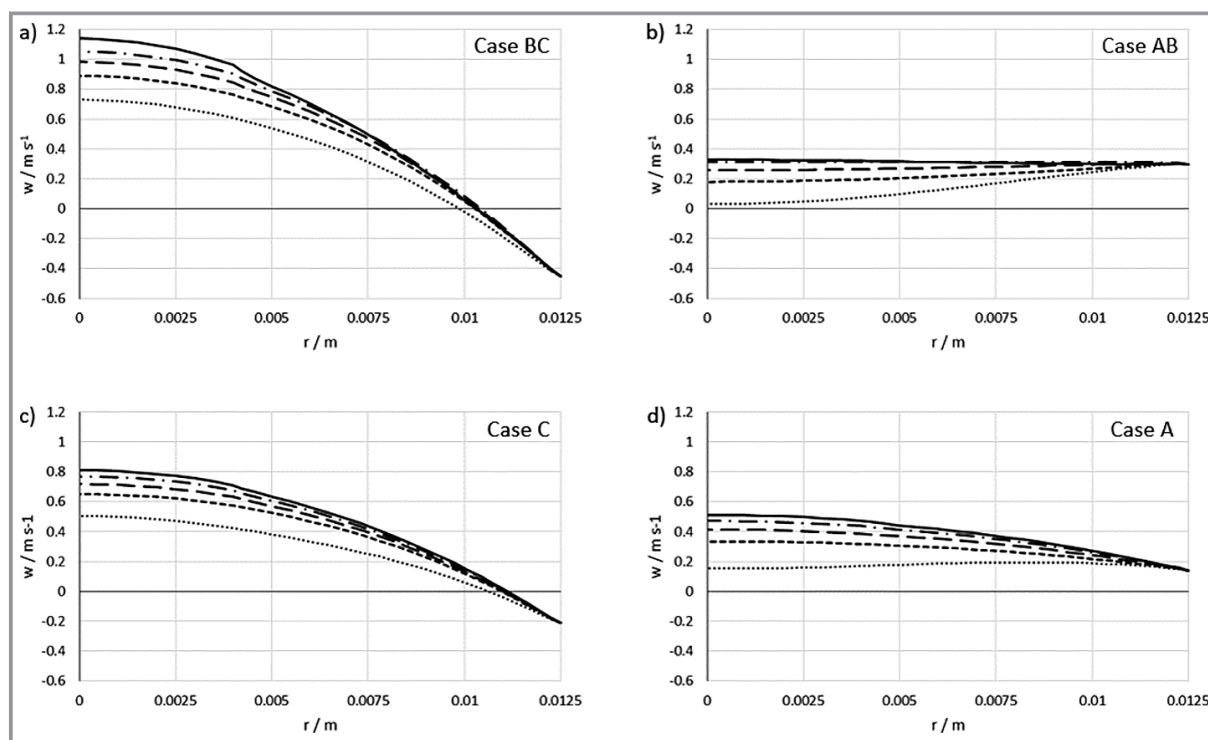


Figure 7. Radial velocity profiles at different locations x along the reactor for different cases. $x = 0$ m to $x = 3$ m corresponds to the range of the reaction zone. (· · ·) $x = 0$ m, (- -) $x = 0.75$ m, (- · -) $x = 1.5$ m, (- - -) $x = 2.25$ m, (-) $x = 3$ m.

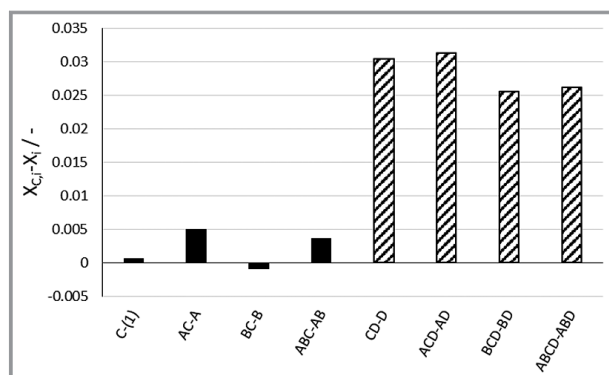


Figure 8. Change in conversion by changing the rotational frequency (black: small diameter; stripes: large diameter).

has a negative effect on the conversion by enhancing the backmixing, while in COC there is an optimum volume flow rate for forming a plug flow. Nevertheless, it is questionable whether setting the optimal volume flow is useful, since a larger volume flow increases the energy required to heat the fluid. Increasing the rotation frequency has a positive effect, especially for larger reactor diameters, because it improves the heat transfer to the center of the reactor. In general, however, increasing the diameter showed conversion losses of more than 10 %.

Furthermore, it could be shown that the increases in conversion due to operating mode, volume flow and rotation frequency are relatively small at a maximum of 4 % in con-

trast to an increase in temperature (Fig. 2). Materials that can withstand higher temperatures should therefore be taken into account in further considerations.

Finally, a comparison with an ideal plug flow reactor was made by averaging the temperature in the reaction zone. Due to non-idealities occurring in the rotating film reactor, a conversion difference of 13 % was found for the highest conversion achieved.

Open access funding enabled and organized by Projekt DEAL.

Symbols used

c	[mol m ⁻³]	concentration
c_p	[J kg ⁻¹ K ⁻¹]	specific heat capacity
d	[m]	wall thickness
E_A	[J mol ⁻¹]	activation energy
$\Delta_i G$	[J mol ⁻¹]	specific Gibbs enthalpy
g	[m s ⁻²]	gravitational factor
H	[J mol ⁻¹]	specific enthalpy
K_C	[mol m ⁻³]	equilibrium constant
k_0	[s ⁻¹ mol ¹⁻ⁿ m ⁻³⁽¹⁻ⁿ⁾]	kinetic constant
L	[m]	length
M	[kg mol ⁻¹]	molar mass

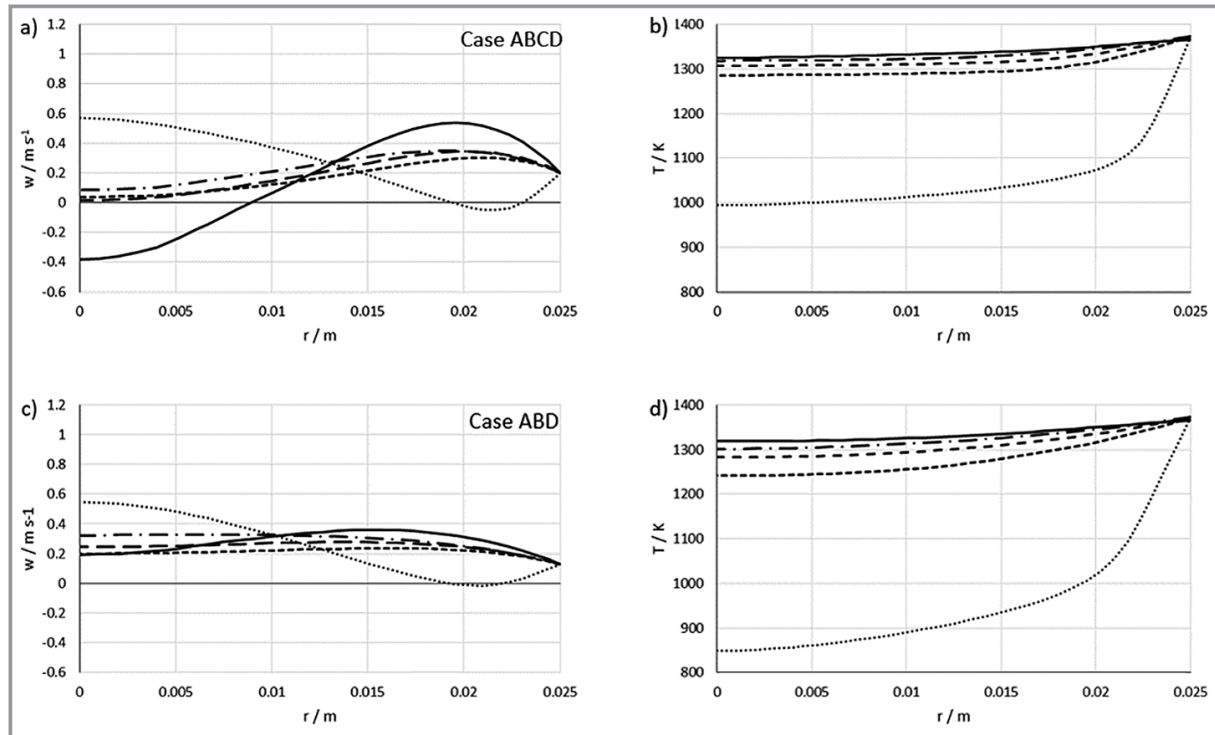


Figure 9. Radial velocity profile and temperature profile at different locations x along the reactor and different rotation frequency. $x = 0$ m to $x = 3$ m corresponds to the range of the reaction zone. (···) $x = 0$ m, (---) $x = 0.75$ m, (-·-) $x = 1.5$ m, (-) $x = 2.25$ m, (- - -) $x = 3$ m.

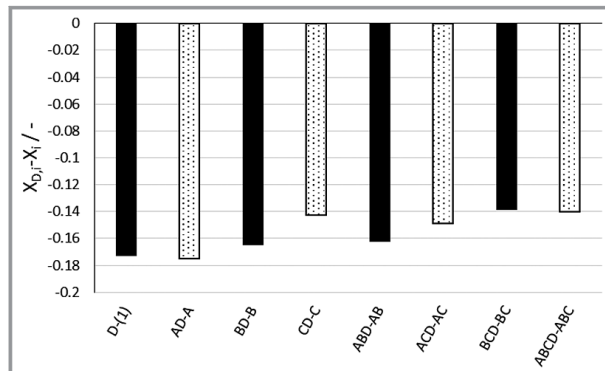


Figure 10. Change in conversion by changing the reactor diameter (black: CTC; dotted: COC).

\dot{m}	[kg m ⁻³]	mass flow rate
n	[-, mol]	reaction parameter, amount of substance
p	[Pa]	pressure
\dot{q}	[W m ⁻³]	heat flux
R	[J K ⁻¹ mol ⁻¹]	universal gas constant
r	[m]	radius
rpm	[min ⁻¹]	rotation frequency
T	[K]	temperature
V	[m ³]	volume
\dot{V}	[m ³ s ⁻¹]	volume flow rate
w	[m s ⁻¹]	axial velocity

x	[m]	axial coordinate
x^*	[-]	dimensionless coordinate
y	[-]	mole fraction

Greek letters

α	[W m ⁻² K ⁻¹]	heat transfer coefficient
β	[-]	temperature exponent
δ	[m]	film thickness
η	[Pa s]	dynamic viscosity
λ	[W m ⁻¹ K ⁻¹]	thermal conductivity
ν	[m ² s ⁻¹]	kinematic viscosity
ρ	[kg m ⁻³]	density
Φ	[mol ⁿ m ⁻ⁿ⁻³]	concentration dependent reaction law
ω	[rad s ⁻¹]	angular velocity
Ψ	[-]	effect in DoE

Sub- and Superscripts

0	initial condition
a	outer
ax	axial
B	box
F	film
fur	furnace

G	gas
i	inner
L	liquid
max	maximum
R	reaction
rot	rotation
W	wall

Abbreviations

CFD	Computational fluid dynamics
COC	Cocurrent flow
CTC	Countercurrent flow
DoE	Design of experiment
PFR	Plug flow reactor

References

- [1] *Hydrogen insights 2021*, Hydrogen Council/McKinsey & Company, Brussels **2021**.
- [2] B. Parkinson, M. Tabatabaei, D. C. Upham, B. Ballinger, C. Greig, S. Smart, E. McFarland, *Int. J. Hydrogen Energy* **2018**, *43* (5), 2540–2555. DOI: <https://doi.org/10.1016/j.ijhydene.2017.12.081>
- [3] O. Machhammer, A. Bode, W. Hormuth, *Chem. Ing. Tech.* **2015**, *87* (4), 409–418. DOI: <https://doi.org/10.1002/cite.201400151>
- [4] T. Keipi, H. Tolvanen, J. Konttinen, *Energy Convers. Manage.* **2018**, *159*, 264–273. DOI: <https://doi.org/10.1016/j.enconman.2017.12.063>
- [5] A. Bode, *Methane pyrolysis – a potential new process for hydrogen production without CO₂ emission*, Niedersächsische Energietage, Hannover, November **2019**.
- [6] J. X. Qian, T. W. Chen, L. R. Enakonda, D. B. Liu, G. Mignani, J.-M. Basset, L. Zhou, *Int. J. Hydrogen Energy* **2020**, *45* (15), 7981–8001. DOI: <https://doi.org/10.1016/j.ijhydene.2020.01.052>
- [7] C. Anjaneyulu, G. Naresh, V. V. Kumar, J. Tardio, T. V. Rao, A. Venugopal, *ACS Sustainable Chem. Eng.* **2015**, *3* (7), 1298–1305. DOI: <https://doi.org/10.1021/acsschemeng.5b00372>
- [8] A. Abánades et al., *Int. J. Hydrogen Energy* **2011**, *36* (20), 12877–12886. DOI: <https://doi.org/10.1016/j.ijhydene.2011.07.081>
- [9] N. Muradov, Z. Chen, F. Smith, *Int. J. Hydrogen Energy* **2005**, *30* (10), 1149–1158. DOI: <https://doi.org/10.1016/j.ijhydene.2005.04.005>
- [10] C. E. Jahnig, P. L. Silveston, C. W. Tyson, *US Patent 2982622*, **1961**.
- [11] M. Steinberg, *Int. J. Hydrogen Energy* **1999**, *24* (8), 771–777. DOI: [https://doi.org/10.1016/S0360-3199\(98\)00128-1](https://doi.org/10.1016/S0360-3199(98)00128-1)
- [12] M. Serban, M. A. Lewis, C. L. Marshall, R. D. Doctor, *Energy Fuels* **2003**, *17* (3), 705–713. DOI: <https://doi.org/10.1021/ef020271q>
- [13] M. Plevan, T. Geißler, A. Abánades, K. Mehravaran, R. Rathnam, C. Rubbia, D. Salmieri, L. Stoppel, S. Stückrad, T. Wetzel, *Int. J. Hydrogen Energy* **2015**, *40* (25), 8020–8033. DOI: <https://doi.org/10.1016/j.ijhydene.2015.04.062>
- [14] T. Geißler et al., *Int. J. Hydrogen Energy* **2015**, *40* (41), 14134–14146. DOI: <https://doi.org/10.1016/j.ijhydene.2015.08.102>
- [15] T. Geißler et al., *Chem. Eng. J.* **2016**, *299*, 192–200. DOI: <https://doi.org/10.1016/j.cej.2016.04.066>
- [16] D. C. Upham, V. Agarwal, A. Khechfe, Z. R. Snodgrass, M. J. Gordon, H. Metiu, E. W. McFarland, *Science* **2017**, *358* (6365), 917–921. DOI: <https://doi.org/10.1126/science.aao5023>
- [17] N. Rahimi, D. Kang, J. Gelinis, A. Menon, M. J. Gordon, H. Metiu, E. W. McFarland, *Carbon* **2019**, *151*, 181–191. DOI: <https://doi.org/10.1016/j.carbon.2019.05.041>
- [18] B. J. L. Pérez, J. A. M. Jiménez, R. Bhardwaj, E. Goetheer, M. van Sint Annaland, F. Gallucci, *Int. J. Hydrogen Energy* **2021**, *46* (7), 4917–4935. DOI: <https://doi.org/10.1016/j.ijhydene.2020.11.079>
- [19] I. Schultz, D. W. Agar, *Int. J. Hydrogen Energy* **2015**, *40* (35), 11422–11427. DOI: <https://doi.org/10.1016/j.ijhydene.2015.03.126>
- [20] A. A. Munera Parra, D. W. Agar, *Int. J. Hydrogen Energy* **2017**, *42* (19), 13641–13648. DOI: <https://doi.org/10.1016/j.ijhydene.2016.12.044>
- [21] T. Becker, F. Keuchel, D. W. Agar, *Chem. Ing. Tech.* **2021**, *93* (5), 762–770. DOI: <https://doi.org/10.1002/cite.202000234>
- [22] K. Kikuyama, M. Murakami, K. Nishibori, K. Maeda, *Bull. JSME* **1983**, *26* (214), 506–513. DOI: <https://doi.org/10.1299/jсме1958.26.506>
- [23] S. Suppiah Singaram, H. Lodha, R. J. Jachuck, *AIChE J.* **2014**, *60* (11), 3939–3950. DOI: <https://doi.org/10.1002/aic.14569>
- [24] L. J. Catalan, E. Rezaei, *Int. J. Hydrogen Energy* **2020**, *45* (4), 2486–2503. DOI: <https://doi.org/10.1016/j.ijhydene.2019.11.143>
- [25] T. Keipi, T. Li, T. Lovås, H. Tolvanen, J. Konttinen, *Energy* **2017**, *135*, 823–832. DOI: <https://doi.org/10.1016/j.energy.2017.06.176>
- [26] K. Siebertz, T. Hochkirchen, D. van Bebbber, *Statistische Versuchsplanung*, Springer, Berlin **2010**.